Postlaunch Calibration of FengYun-3B MERSI Reflective Solar Bands

Ling Sun, Xiuqing Hu, Na Xu, Jingjing Liu, Lijun Zhang, and Zhiguo Rong

***Abstract*—The MEdium Resolution Spectral Imager (MERSI) is the keystone instrument onboard FengYun-3 (FY-3). After FY-3A, FY-3B MERSI is the second launched in November 2010. Nineteen of the 20 MERSI spectral bands are the reflective solar bands, which cannot be absolutely calibrated onboard. The annual vicarious calibration (VC) based on synchronous *in situ* measurements at the Dunhuang site is the baseline calibration method for MERSI. To assure frequent and stable calibration updates, a multisite calibration tracking method is developed. This paper presents the FY-3B MERSI postlaunch daily calibration updating method based on multisite calibration tracking with the Dunhuang VC correction, the long-term sensor response on-orbit change, and the calibration performance evaluation. A reflectance-based method is used for the Dunhuang VC, and the reflectance calibration uncertainties are within 3% for most MERSI bands. The multisite calibration tracking method relies on simulated radiation over several stable sites without synchronous *in situ* measurements. A postlaunch daily calibration updating model is established using a linear function of days since launch to describe the long-term trend. The calibration updating model is validated by the Dunhuang VC, showing the relative bias within 3.5% for most bands. It is found that the shortwave channels of MERSI experience large degradation, particularly the 412-nm band with an annual degradation rate of approximately 18%, whereas most red and near-infrared bands are relatively stable. Using the calibration updating model with the Dunhuang VC correction, the recalibrated MERSI data are validated against Moderate Resolution Imaging Spectroradiometer by near synchronous-nadir-observation analysis, and good agreement is achieved.**

***Index Terms*—Dunhuang site vicarious calibration (VC), FY-3B MEdium Resolution Spectral Imager (MERSI), multisite calibration tracking, on-orbit response change, reflective solar bands (RSBs).**

I. Introduction

THE FengYun-3 (FY-3) series is the second generation of Chinese polar-orbit meteorological satellites [1]. After FY-3A, FY-3B is the second spacecraft launched on November 5, 2011, in a near-sun-synchronous polar orbit with a nominal altitude of 836 km and an equatorial crossing time of 1:30 P.M. (ascending northward). MEdium Resolution Spectral Imager (MERSI) is a keystone payload onboard FY-3, containing 20 bands covering the spectral range from visible (VIS) to long-wave infrared (LWIR). The nadir spatial resolutions are 0.25 km (five bands) and 1 km (15 bands). FY-3 MERSI is capable of making global observations for a broad range of scientific studies of Earth's system.

Radiometric calibration is one of the prerequisites of successful quantitative remote sensing applications. The experience of Moderate Resolution Imaging Spectroradiometer (MODIS) reveals that the long-term on-orbit response changes are relatively large at visible spectral bands, particularly shortwave bands with wavelengths less than 500 nm [2], which must be effectively monitored and corrected to assure the science product quality. Earth Observing System MODIS is a generally accepted Earth-observing sensor with stable performance and good calibration accuracy. Based on the complex onboard calibrators (OBCs), MODIS realizes the on-orbit absolute calibration using onboard solar diffuser (SD) and an SD stability monitor. In addition, regularly scheduled lunar observations are made to track the reflective solar band (RSB) calibration stability [2]. Although FY-3 MERSI is a high-quality civil instrument in China, it still cannot realize the RSB onboard absolute radiometric calibration. Other calibration approaches must be taken to achieve the expected calibration accuracy requirement of 7% for RSBs. There are already many postlaunch calibration and monitoring methodologies in the solar reflective spectral region, including uniform-site-based vicarious calibration (VC) using radiative transfer models (RTMs) with input parameters from synchronous *in situ* measurements (e.g., [3] and [4]) or other sources (e.g., [5]–[7]); "invariant" target tracking such as bright desert (e.g., [5], [6], [8], and [9]), glaciers (e.g., [10] and [11]), and deep convective cloud (e.g., [12] and [13]), as well as the moon (e.g., [14] and [15]); and intercalibration based on a reference sensor or band (e.g., [16] and [17]). In general, based on the long-term tracking analysis of stable targets on Earth's surface, in the atmosphere, or even in the outer space, the sensor response change could be monitored relative to a reference moment. However, without reliable onboard calibration, the site VC with synchronous *in situ* measurements is still the main choice for absolute calibration at the reference moment.

China Radiometric Calibration Site (CRCS) for satellite sensor calibration for RSBs is located in the Dunhuang Gobi desert in northwest China. The Dunhuang VC based on synchronous *in situ* measurements has been the baseline calibration approach for Chinese FY series satellites since 2002, and an annual field campaign has been routinely carried out in summer [18]. The limited frequency of once a year is not enough for frequent and stable on-orbit calibration-coefficient updating. To increase the postlaunch calibration frequency and monitor the radiometric response change of MERSI, a multisite calibration tracking method based on stable targets and radiative transfer modeling

Manuscript received February 17, 2012; revised July 3, 2012; accepted August 10, 2012. Date of publication October 22, 2012; date of current version February 21, 2013. This work was supported in part by the National Key Basic Research Science Foundation of China under Contract 2010CB950802 and Contract 2010CB950803 and in part by the Meteorological Special Project under Contract GYHY200906036.

The authors are with the National Satellite Meteorological Center, China Meteorological Administration, Beijing 10081, China (e-mail: sunling@cma.gov.cn).

Digital Object Identifier 10.1109/TGRS.2012.2217345

TABLE I
MERSI SPECTRAL BAND SPECIFICATIONS

Band	CW (μm)	BW (μm)	IFOV (m)	NEΔρ(%) or NEΔT(K@300K)	Dynamic Range (maximum ρ or T)
1	0.470	0.05	250	0.3	100%
2	0.550	0.05	250	0.3	100%
3	0.650	0.05	250	0.3	100%
4	0.865	0.05	250	0.3	100%
5	11.25	2.5	250	0.4K	330K
6	1.640	0.05	1000	0.08	90%
7	2.130	0.05	1000	0.07	90%
8	0.412	0.02	1000	0.1	80%
9	0.443	0.02	1000	0.1	80%
10	0.490	0.02	1000	0.05	80%
11	0.520	0.02	1000	0.05	80%
12	0.565	0.02	1000	0.05	80%
13	0.650	0.02	1000	0.05	80%
14	0.685	0.02	1000	0.05	80%
15	0.765	0.02	1000	0.05	80%
16	0.865	0.02	1000	0.05	80%
17	0.905	0.02	1000	0.10	90%
18	0.940	0.02	1000	0.10	90%
19	0.980	0.02	1000	0.10	90%
20	1.030	0.02	1000	0.10	90%

CW: Central wavelengths; BW: Bandwidths;
IFOV: Instantaneous field of view (nadir).

without synchronous *in situ* measurements has been developed. The FY-3B MERSI postlaunch daily calibration updating model is thus established based on the multisite calibration tracking with the Dunhuang VC correction. The objective of this paper is to present the FY-3B MERSI RSB postlaunch daily calibration updating method, the long-term sensor response on-orbit change, and the calibration performance. Following a brief sensor overview in Section II, the Dunhuang VC method and result for FY-3B MERSI RSBs, as well as the calibration reference uncertainty evaluation with respect to Aqua MODIS, are described in Section III. Section IV demonstrates the multisite calibration tracking method without synchronous *in situ* measurements. Based on the calibration-coefficient trending analysis, the long-term sensor response on-orbit change is revealed, and the postlaunch daily calibration updating model is established. The Dunhuang VC result is then used for the correction of the postlaunch daily calibration updating model. Provided in Section V are the evaluation of FY-3B MERSI calibration performance with respect to Aqua MODIS. The usability of the prelaunch calibration coefficients is also analyzed. Section VI is a summary of this paper.

II. FY-3B MERSI OVERVIEW

MERSI was built by Shanghai Institute of Technical Physics, Chinese Academy of Sciences. It has 19 RSBs with wavelengths from 0.41 to 2.13 μm and one thermal emissive band (TEB) with a wavelength at 11.25 μm. For reference purposes, Table I provides the spectral band specifications, and Fig. 1 shows the RSB spectral response functions (SRFs). MERSI is a cross-track scanning radiometer, which collects data using a 45° single-sided scan mirror and a two-sided derotated K mirror. There are totally 350 along-track detectors, 40 and 10 detectors for each 0.25-km (bands 1–5) and 1-km (bands 6–20) spatial-resolution band, respectively. It produces a swath of 2900-km cross-track by 10-km (at nadir) along-track each 1.5-s scan with a wide field of view (FOV) of $\pm 55^\circ$ from instrument nadir. This enables the complete global coverage in one day.

The expected calibration accuracy requirement of RSBs is 7%. MERSI has two OBCs, including a blackbody (BB) for TEB on-orbit calibration and a visible OBC (VOC) for RSBs. MERSI VOC is an onboard visible calibration experimental device. It is composed of a 6-cm diameter integrating sphere with two interior halogen-tungsten lamps and a sunlight import cone, an export beam expanding system with a flat mirror and a parabola to create a quasi-Gaussian beam, and absolute radiance trap detectors (four detectors with the same filter designs as MERSI bands 1–4 and one panchromatic detector with no filter). The MERSI VOC is only used for tracking the temporal instrument degradation for research purposes because of its nonregular operation and inability to be traced back to a prelaunch standard. The space view (SV), Earth view (EV), VOC, and BB are observed in each scan.

The detector uniformity brings strips in the original MERSI image. Based on the linear correction coefficients from prelaunch measurements, detector outputs are normalized to the reference one onboard before data downlink. The remaining strips are recorrected using lookup tables from global-scene-based histogram matching.

The shortwave-infrared (SWIR; bands 6 and 7) and the LWIR (band 5) focal plane assemblies should be cooled to approximately 90 K by a passive radiant cooler. Unfortunately, the antifouling cover of space radiant cooler was not successfully opened. Thus, bands 6 and 7 are operated in anomalous working conditions without temperature control since January 21, 2011, and band 5 is inoperable.

III. DUNHUANG SITE VC

The Dunhuang test site, i.e., the CRCS for the Chinese satellite sensor calibration for RSBs, was selected in 2008 by the Working Group on Calibration and Validation (WGCV) of the Committee on Earth Observation Satellites (CEOS) as one of the instrumented reference sites. It is located on a stable alluvial fan whose surface consists of cemented gravel with some gray or black stones and almost no vegetation. The surface spectral reflectance is temporally stable, and the coefficient of variation (CV), defined as the ratio of standard deviation (Std) over average (Mean), is approximately 3% over the 10 km $\times$ 10 km central region. The aerosol loading is low, with an average optical depth of approximately 0.2 at 550 nm, except during the dusty spring season. The surface reflectance is approximately 15%–30% in the visible and near-infrared spectral regions, and the surface bidirectional reflectance distribution function (BRDF) was modeled with field measurements in summer 2008 [18].

The CRCS VC based on synchronous *in situ* measurements has been the baseline calibration approach for Chinese FY series satellites since 2002. The reflectance-based method is used for RSB calibration. Field campaigns have been routinely carried out once a year in summer, in which surface spectral reflectance, aerosol optical property, and atmospheric profile are synchronously measured with the satellite overpass (within 1 h). The first CRCS field campaign for FY-3B MERSI was carried out in August 2011.

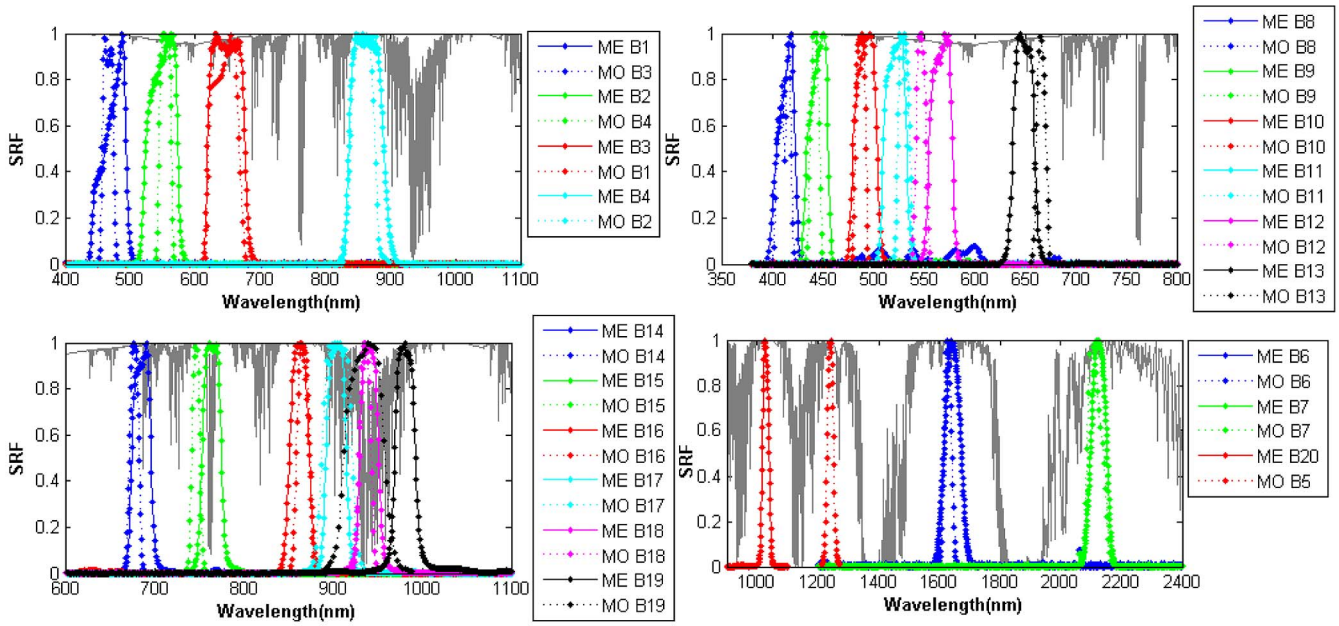

Fig. 1. Spectral response functions of FY-3B MERSI RSBs with Aqua MODIS overplots. The gaseous absorption transmittance is shown with shaded black line.

A. Calibration Method

The *in situ* measured parameters at Dunhuang are input to RTMs, and the calibration coefficients (slopes) are obtained using the simulated top-of-the-atmosphere (TOA) apparent reflectance and MERSI observations of EV and SV by

$$100\mathrm{Ref}_i \cos(\mathrm{SolZ})/d^2 = \mathrm{Slope}_i(\mathrm{EV}_i - \mathrm{SV}_i) \qquad (1)$$

where Ref_i is the RTM calculated instantaneous TOA reflectance for band i, SolZ is the solar zenith angle, d is the Earth–sun distance in AU, Slope is the calibration slope, and EV and SV are digital counts of Earth and SV observations (taken as the radiation zero reference), respectively. In the following, $\mathrm{Ref}_i \cos(\mathrm{SolZ})/d^2$ is denoted as the reflectance factor (RefFactor).

6SV 1.0 and MODTRAN 4.0 are adopted as the radiative transfer codes to calculate the TOA reflectance. The vector model 6SV is mainly used for scattering calculation, while the gaseous absorption transmittance from MODTRAN is used to correct the lower estimation from 6SV.

The Ångström wavelength exponents of continental and background-desert aerosol models contained in 6SV are about 1.2 and 0.3, respectively. Considering the fact that the measured exponent during each Dunhuang site VC campaign usually varies between 0.3 and 1.3, the aerosol model is dynamically chosen according to the *in situ* measured Ångström exponent as the continental model (Ångström > 0.75) or desert model (Ångström ≤ 0.75).

The surface bidirectional reflectance model adopts the MODIS BRDF model Algorithm for Model Bidirectional Reflectance Anisotropies of the Land Surface (AMBRALS) with the following expression:

$$\begin{aligned} &R(\mathrm{SenZ}, \mathrm{SolZ}, \mathrm{RelA}, \lambda) \\ &\quad = \mathrm{Par}_1(\lambda) + \mathrm{Par}_2(\lambda) k_{\mathrm{vol}}(\mathrm{SenZ}, \mathrm{SolZ}, \mathrm{RelA}) \\ &\qquad + \mathrm{Par}_3(\lambda) k_{\mathrm{geo}}(\mathrm{SenZ}, \mathrm{SolZ}, \mathrm{RelA}) \end{aligned} \qquad (2)$$

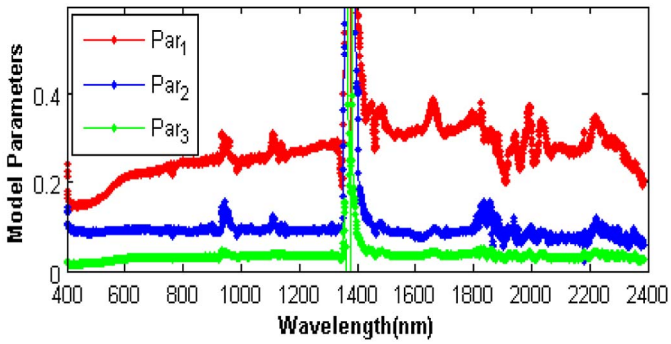

Fig. 2. BRDF model parameters of the Dunhuang surface from *in situ* measurement in 2008.

TABLE II
PARAMETERS FOR FY-3B MERSI DUNHUANG SITE CALIBRATION IN AUGUST 2011

Date	$\tau_a(550)$	Ångström	Water Vapor (g/cm^2)	SolZ (°)	SenZ (°)	RelA (°)
Aug. 18	0.085	1.210	2.026	33.798	39.543	39.330
Aug. 24	0.138	1.140	1.300	34.027	22.590	-43.253
Aug. 25	0.134	1.079	0.799	32.362	7.261	-229.837
Aug. 30	0.170	0.776	2.243	34.651	1.742	-41.664

where $R(\mathrm{SenZ}, \mathrm{SolZ}, \mathrm{RelA}, \lambda)$ is the BRDF, SolZ is the solar zenith angle, SenZ is the view zenith angle, RelA is the view-solar relative azimuth angle, λ is the wavelength, $k_{\mathrm{vol}}(\mathrm{SenZ}, \mathrm{SolZ}, \mathrm{RelA})$ is the RossThick kernel, $k_{\mathrm{geo}}(\mathrm{SenZ}, \mathrm{SolZ}, \mathrm{RelA})$ is the LiSparse-R kernel, and $\mathrm{Par}_1(\lambda)$, $\mathrm{Par}_2(\lambda)$, and $\mathrm{Par}_3(\lambda)$ are the BRDF kernel model parameters representing the weights of isotropic scattering, volume scattering, and geometry optical scattering, respectively. The BRDF model parameters are wavelength dependent, and the *in situ* model at Dunhuang obtained in summer 2008 is used [18] (see Fig. 2).

Because the *in situ* BRDF model at Dunhuang is built using measurements only in 2008, the model parameters must be

TABLE III
FY-3B MERSI CALIBRATION SLOPES FROM DUNHUANG SITE CALIBRATION IN AUGUST 2011

Band / Date	1	2	3	4	6	7	8	9	10	11	12	13	14	15	16	17	18	19	20
Aug. 18	0.0306	0.0301	0.0284	0.0300	0.0227	0.0179	0.0281	0.0254	0.0230	0.0227	0.0226	0.0225	0.0199	0.0210	0.0231	0.0238	0.0206	0.0254	0.0290
Aug. 24	0.0304	0.0297	0.0279	0.0287	0.0216	0.0169	0.0278	0.0252	0.0228	0.0224	0.0225	0.0219	0.0194	0.0205	0.0221	0.0227	0.0203	0.0239	0.0273
Aug. 25	0.0302	0.0293	0.0269	0.0276	0.0222	0.0174	0.0276	0.0250	0.0225	0.0222	0.0220	0.0211	0.0187	0.0197	0.0213	0.0226	0.0222	0.0232	0.0261
Aug. 30	0.0307	0.0299	0.0277	0.0288	0.0225	0.0175	0.0281	0.0255	0.0229	0.0226	0.0224	0.0218	0.0193	0.0205	0.0223	0.0225	0.0186	0.0238	0.0274
Mean	0.0304	0.0296	0.0275	0.0284	0.0221	0.0173	0.0278	0.0252	0.0227	0.0224	0.0223	0.0216	0.0191	0.0202	0.0219	0.0226	0.0204	0.0236	0.0270
CV(%)	0.7254	1.0673	1.843	2.3706	2.1366	1.7371	0.8789	0.9134	0.9668	1.0473	1.2689	1.9494	2.0571	2.2866	2.3241	0.4601	8.7557	1.5702	2.6395

Mean and CV(%) are calculated using data with SenZ<30°.

corrected according to the real-time *in situ* surface reflectance and convolved using SRFs for each band by

$$\begin{aligned}\mathrm{Par}'(\lambda) &= \mathrm{Par}(\lambda)\mathrm{Factor}(\lambda) \\ &= \mathrm{Par}(\lambda)R_{\text{in-situ}}(\lambda)/R_{\text{model}}(\text{SenZ, SolZ, RelA},\lambda)\end{aligned} \tag{3}$$

$$\mathrm{Par}_i = \sum \mathrm{SRF}_i(\lambda)\mathrm{Par}'(\lambda)E_s(\lambda)/\left(\sum \mathrm{SRF}_i(\lambda)E_s(\lambda)\right) \tag{4}$$

where $\mathrm{Par}(\lambda)$ and $\mathrm{Par}'(\lambda)$ are the original and corrected model parameters at wavelength λ, "Factor" is the correction factor, $R_{\text{in-situ}}$ and R_{model} are the *in situ* surface reflectance (collected within 1 h around satellite overpass) and the BRDF model estimation under the same viewing geometry as the *in situ* one, SRF_i is the SRF for band i, E_s is the solar irradiance at TOA, and Par_i is the band equivalent value for band i.

Other atmospheric parameters input to the RTM consist of the aerosol optical thickness at 550-nm $\tau_a(550)$, which takes the measurement average within half an hour around the satellite overpass, the atmospheric profile taken from the sounding measurement by Dunhuang national climatic observation station within an hour around the satellite overpass, and the ozone column amount taken from the Ozone Monitoring Instrument daily product.

The average values around the site center are selected as the matched satellite data using the following criteria: data in 3×3 pixel box centered at the nearest pixel to site center (40.138° N, 94.321° E) are taken; if the distance from the nearest pixel to site center is larger than 0.01°, data are discarded; the average and Std are calculated for the 3×3 box; and if the CV is larger than 1% at band 2 (550 nm), data are discarded.

B. Calibration Result

There are four matched data set for FY-3B MERSI during the Dunhuang VC campaign in August 2011, and the atmospheric and angle parameters are listed in Table II. Table III gives the VC results. Good agreement exists among calibration slopes of individual days. The CV values are less than 3% (except for band 18 at 940 nm strongly affected by water-vapor absorption) when viewing zenith angles less than 30°. Because bands 6 and 7 operate at an abnormal working state without radiative cooling and the uncertainty in water-vapor measurements is relatively large, the calibration results for bands 6, 7, and 18 are just for reference.

C. MODIS-Based Calibration Evaluation

MODIS is the well-calibrated stable sensor, and since the RSB on-orbit performance of Aqua MODIS is better than that of Terra MODIS [2], Aqua MODIS is used as the reference to evaluate the MERSI Dunhuang VC reference, i.e., simulated TOA reflectance. The MODIS TOA reflectance simulated by RTMs at Dunhuang using the same calculation scheme for MERSI is compared with sensor measurement.

TABLE IV
PARAMETERS FOR AQUA MODIS DUNHUANG SITE CALIBRATION IN AUGUST 2011

Date	$\tau_a(550)$	Ångström	Water Vapor (g/cm^2)	SolZ(°)	SenZ(°)	RelA(°)
Aug. 18	0.082	1.215	2.026	34.464	50.731	-39.230
Aug. 22	0.276	0.406	1.681	32.657	18.202	-44.070
Aug. 24	0.144	1.109	1.300	32.066	4.420	-229.750
Aug. 26	0.137	0.991	1.130	31.689	25.800	-233.128

The version 5 products of MYD1KM and MYD03 are obtained from the National Aeronautics and Space Administration during the Dunhuang VC campaign in August 2011. The same scheme as MERSI is used to obtain the TOA reflectance, except that the CV threshold used in satellite data selection is 1.5% for band 4 (555 nm). There are four matched data sets for Aqua MODIS, and Table IV lists the atmospheric and angle parameters. Because MODIS is usually saturated in bands 11 to 16 at Dunhuang and bands 18, 19, and 26 are strongly affected by water-vapor absorption, the comparison analysis is only performed for the first ten bands and band 17 with the central wavelengths at 645, 858, 469, 555, 1240, 1640, 2130, 412, 443, 490, and 905 nm, respectively.

Table V lists the relative bias in percent between simulated Aqua MODIS TOA apparent reflectance and sensor measurements, defined as $100(\mathrm{Ref}^{\mathrm{Est}} - \mathrm{Ref}^{\mathrm{Mea}})/\mathrm{Ref}^{\mathrm{Mea}}$. It shows that the simulated reflectance tends to be overestimated for bands 1, 3, 4, 7, 8, 9, and 17, while it tends to be underestimated for band 2; the differences are almost within 4% for window bands at the visible and near infrared with wavelengths less than 1 μm, with the exception of bands 8 (412 nm) and 7 (2.1 μm). The reason for the relative large bias at band 8 is mainly due to the aerosol model sensitivity at short wavelength.

IV. MULTISITE CALIBRATION TRACKING

Although the Dunhuang synchronous-measurement-based VC could meet the calibration requirement of 4% for most bands, the limited frequency of once a year is not enough for frequent and stable on-orbit calibration-coefficient updates. To increase the calibration frequency, a calibration tracking method has been used to monitor the RSB radiometric response variation, which is based on stable targets and radiative transfer modeling without synchronous *in situ* measurements.

TABLE V
RELATIVE BIAS IN PERCENT BETWEEN SIMULATED AQUA MODIS TOA APPARENT REFLECTANCE AND SENSOR MEASUREMENTS

Band / Date	1	2	3	4	5	6	7	8	9	10	17
Aug. 18	3.85	1.89	3.59	3.71	3.31	3.05	10.06	4.45	1.64	1.07	6.77
Aug. 22	3.26	-0.71	2.88	4.15	0.89	*	8.75	7.65	2.36	0.30	3.59
Aug. 24	2.43	-1.55	1.56	3.24	-1.81	*	6.00	4.61	0.41	-0.05	5.00
Aug. 26	-0.11	-4.51	2.71	2.83	-3.80	*	6.88	4.40	1.98	1.16	2.72
Mean	1.86	-2.25	2.38	3.41	-1.58	*	7.21	5.56	1.58	0.47	3.77
Std	1.75	2.00	0.72	0.67	2.36	*	1.41	1.82	1.03	0.63	1.15

*: Bad detector exists.
Mean and Std are calculated using data with SenZ<30°.

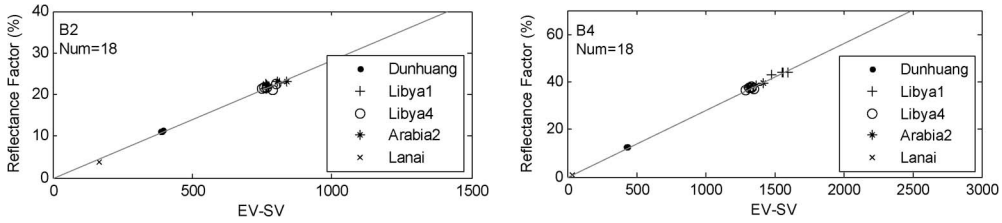

Fig. 3. Typical scatter diagrams of simulated TOA reflectance versus MERSI EV digital number with SV subtracted for MERSI bands 2 and 4. The 18 data points are acquired between day number since launch 80 and 90.

For FY-3B MERSI, multiple sites with uniform and stable surface properties have been chosen for radiometric calibration tracking. Three bright desert target sites, namely, Libya1 (24.42° N, 13.35° E), Libya4 (28.55° N, 23.39° E), and Arabia2 (20.13° N, 50.96° E), and one Gobi desert site, i.e., Dunhuang (40.14° N, 94.32° E), with medium brightness as recommended by CEOS/WGCV, are chosen, as well as a dark ocean site at Lanai (20.49° N, −157.11° E) with Marine Optical Buoy (MOBY) measurements [19].

A. Calibration-Coefficient Series Without In Situ Measurements

Average values in a 3 × 3 box around the site center are selected as the matched satellite data. A similar scheme, as described in Section III, is used to calculate the TOA reflectance, except that no *in situ* measurements are used. The surface bidirectional reflectance of land sites is represented using the MODIS BRDF model [20]. This BRDF model depends on three kernel model parameters that are wavelength dependent. Parameters taken from MCD43C1 products are spectrally interpolated to the central wavelengths of MERSI bands. Water-leaving reflectance is taken from MOBY measurements for the ocean site. A US1962 vertical atmospheric profile is assumed all year long. The desert and maritime aerosol models provided in 6SV are assumed for land and ocean sites, respectively. The aerosol optical depth at 550 nm is taken from the MODIS monthly aerosol product (Aqua Deep Blue result for land and Terra result for ocean) [21]. The total column ozone is taken from a monthly mean climate data set that is generated from several years of Total Ozone Mapping Spectrometer observations [22], and the total column water vapor and surface wind speed are taken from a climatology monthly mean from the National Center for Environmental Prediction analyzed data [23].

In general, the calibration coefficient slowly changes with time. Considering that data from multiple sites with different brightness values could achieve a better coverage of sensor dynamic range than one site and a large amount of data could permit the reduction of calibration errors mainly due to calculated reflectance uncertainties, the calibration coefficient is calculated based on the acquisition of data during an accumulation period and from the five sites with (1). In this paper, a ten-day period is selected as the calibration time interval. Cloud-contaminated data are discarded if the relative bias between MERSI measured TOA reflectance and RTM simulation exceeds 50%. Because the sensor response degradation of the near-infrared band is small, as described in Section IV-B, band 4 (865 nm) and Dunhuang VC coefficients given in Section III are used. Fig. 3 displays the typical calibration scatter diagrams with an accumulation period of ten days when the sensor zenith angle is below 50° and the solar zenith angle is below 60°.

B. Calibration-Coefficient Varying Trend

Based on the calibration-coefficient series, a linear model is used to describe the long-term varying trend of calibration slopes by

$$\text{Slope}_i = a_i \text{DSL} + b_i \tag{5}$$

where DSL is the number of days since launch, and a_i and b_i are coefficients for band i. Fig. 4 shows the typical calibration slope time series for bands 1–4 using data from November 2010 to December 2011, in which the linear regression model is shown by a solid black line and the VC result at Dunhuang in August 2011 is shown by blue squares. It can be seen that the calibration coefficients present a linear varying trend with DSL, but a seasonal periodicity still exists in some bands. The calibration coefficients could be estimated for each day by using the linear fitting parameters. Table VI lists the relative bias between the estimated calibration coefficients and those from Dunhuang VC in August 2011. It shows that the relative bias are within 3.5% for most bands with the exception of bands 8 (412 nm), 6 (1.6 μm), and 7 (2.1 μm). Surface property is the largest factor

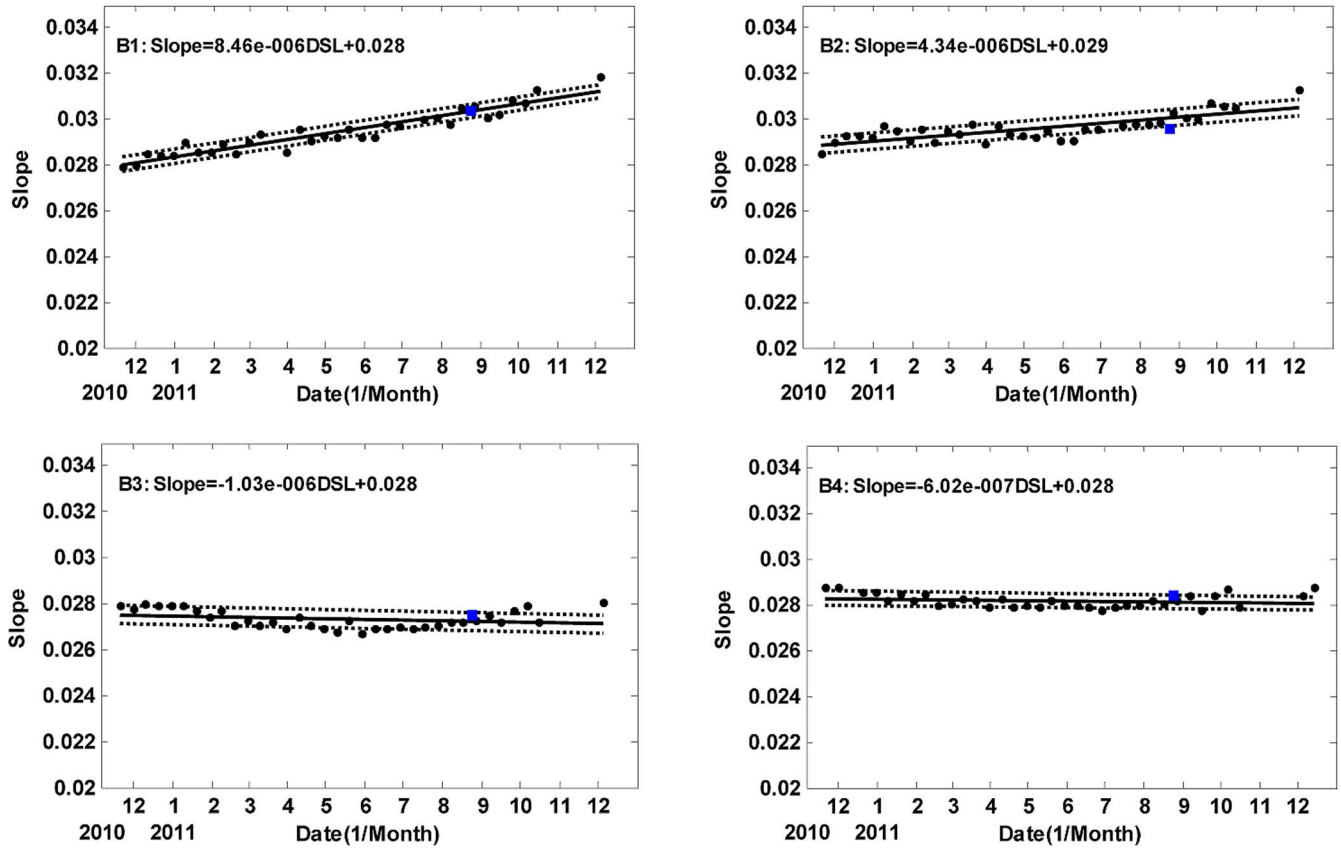

Fig. 4. (Dots) Calibration slope time series for bands 1 to 4 from multisite calibration tracking from November 2010 to December 2011. (Solid Line) The time variation of calibration slopes exhibits regular changes that can be fitted with a linear model. (Dashed line) One Std of the difference between the calibration slopes and estimations from the fitting model. (Blue square) VC result at Dunhuang in August 2011.

TABLE VI
CALIBRATION SLOPE RELATIVE BIAS BETWEEN ESTIMATION USING MULTISITE METHOD AND 2011 DUNHUANG VICARIOUS CALIBRATION

Band	PDif (%)	Band	PDif (%)
1	-0.07	12	-1.59
2	1.65	13	0.07
3	-0.96	14	2.26
4	-0.86	15	2.59
6	6.47	16	0.96
7	7.87	17	2.30
8	-5.90	18	-3.49
9	-0.29	19	2.63
10	2.80	20	2.39
11	3.44		

PDif=(Slope$_{\text{Multi-site}}$-Slope$_{\text{Dunhuang}}$)/Slope$_{\text{Dunhuang}}$.

TABLE VII
PARAMETERS OF FY-3B MERSI DAILY CALIBRATION UPDATING MODEL FROM MULTISITE METHOD AFTER DUNHUANG VC CORRECTION

Band	a	b	2σ/Mean (%)
1	8.46E-06	0.0279	2.01
2	4.34E-06	0.0283	2.31
3	-1.03E-06	0.0278	2.81
4	-6.02E-07	0.0286	2.07
6	9.79E-07	0.0218	12.42
7	-2.80E-06	0.0181	14.57
8	1.38E-05	0.0235	2.83
9	1.14E-05	0.0219	2.42
10	5.54E-06	0.0211	2.92
11	3.33E-06	0.0215	3.01
12	1.35E-06	0.0219	2.27
13	-7.09E-08	0.0216	2.93
14	-1.66E-07	0.0191	2.33
15	-1.33E-06	0.0206	2.88
16	-2.46E-07	0.0220	1.47
17	1.38E-06	0.0222	4.60
18	5.03E-06	0.0189	12.72
19	3.30E-06	0.0227	4.17
20	5.57E-06	0.0254	1.32

σ: The standard deviation of difference between calibration slopes and estimations from the linear regression model.
Mean: The average value of the estimations from the linear model.

to affect the calibration performance. The spectral interpolation of BRDF model parameters from MCD43 will introduce error. It is clear that, for the first four bands whose bands are similar as MODIS, the relative biases are less than 2%. Except for the two SWIR bands working in abnormal conditions, band 8 (412 nm) with the shortest wavelength exhibits the largest difference because it is more influenced by the uncertainty of aerosol.

The calibration coefficients from Dunhuang VC in August 2011 (DSL = 293) Slope$_{\text{VC}}$ is used to correct the model estimated initial calibration slope b_i at launch day (DSL = 0) by

$$b_i' = \text{Slope}_{\text{VC}} b_i / (a_i \text{DSL} + b_i). \quad (6)$$

Table VII lists the parameters of the daily calibration updating model after the Dunhuang VC correction. The uncertainty $(2\sigma/\text{mean}(\%))$ of the slope trend analysis is less than 3% for

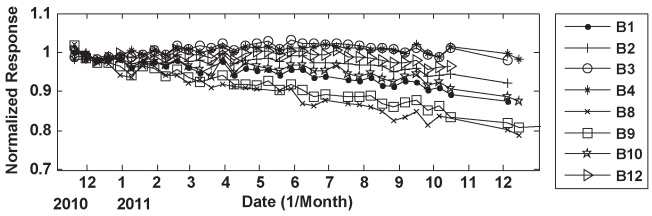

Fig. 5. Time series of normalized response from November 2010 to December 2011.

TABLE VIII
FY-3B MERSI RSB RESPONSE DEGRADATION TREND ANALYSIS RESULTS

Band	c	d	2σ/Mean (%)	Annual Degradation Rate (%)
1	-2.69E-04	0.9976	2.01	9.84
2	-1.40E-04	0.9992	2.31	5.13
3	3.78E-05	1.0002	2.81	-1.38
4	2.14E-05	1.0001	2.07	-0.78
8	-4.98E-04	0.9920	2.83	18.33
9	-4.25E-04	0.9931	2.42	15.62
10	-2.27E-04	0.9978	2.92	8.31
11	-1.38E-04	0.9990	3.01	5.06
12	-6.01E-05	0.9999	2.27	2.20
13	3.52E-06	1.0002	2.93	-0.13
14	8.80E-06	1.0001	2.33	-0.32
15	6.37E-05	1.0003	2.88	-2.32
16	1.12E-05	1.0000	1.47	-0.41
17	-5.98E-05	1.0005	4.60	2.18
18	-2.47E-04	1.0017	12.72	9.00
19	-1.33E-04	0.9997	4.17	4.86
20	-1.95E-04	0.9984	1.32	7.13

almost all bands except for two SWIR bands 6 and 7, and bands 17–19 affected by water vapor.

C. Response Degradation Trending

The normalized response for band i is defined as $m_i = b_i/\text{Slope}_i$. The normalized response is also linearly fitted using

$$m_i = c_i \text{DSL} + d_i \tag{7}$$

where c and d are degradation model coefficients. Thus, the annual degradation rate of the sensor response could be determined through

$$\text{AnnualRate}_i = -365 c_i / d_i. \tag{8}$$

Fig. 5 presents the normalized response time series. Table VIII lists the response degradation trend analysis results (bands 6 and 7 are omitted). It reveals that the response changes are wavelength dependent. Bands with central wavelengths less than 600 nm have an obvious degradation, particularly band 8 (412 nm) with an annual degradation rate of approximately 18%; bands with wavelengths longer than 900 nm also show a noticeably response decrease, particularly band 20 (1.03 μm) with an annual degradation rate of approximately 7%. Most red and near-infrared bands (600–900 nm) are relatively stable with annual degradation rates within $\pm 1\%$ except for bands 3 (650 nm) and 15 (765 nm), which have noticeably response increase over 1% per year.

V. ANALYSIS AND DISCUSSION

A. Postlaunch Calibration Updating Evaluation Based on MODIS

FY-3B MERSI calibration coefficients are updated every day using the calibration updating model given in Section IV-B through (5) with the parameters listed in Table VII. Aqua MODIS is used as the reference to evaluate the performance of the MERSI daily calibration updating model. The recalibrated MERSI TOA reflectance is cross-compared with Aqua MODIS measurement using a near-synchronous-nadir-observation (SNO) method. The version 5 products of MYD1KM and MYD03 are used when the nadir overpass time differences from FY-3B MERSI are within 5 min. Data are mapped in 1024×1024 using Lambert projection centered at nadir. The following criteria are used in MERSI and MODIS satellite data matching: angle requirement of $\text{SenZ} < 35^\circ$, $|\cos(\text{SenZ}_{\text{MODIS}})/\cos(\text{SenZ}_{\text{MERSI}}) - 1| < 0.01$, and $|\cos(\text{SolZ}_{\text{MODIS}})/\cos(\text{SolZ}_{\text{MERSI}}) - 1| < 0.01$; and space uniformity requirement of $\text{CV} < 2\%$ and $\text{Std} < 0.1\%$ in each 3×3 box.

Fig. 1 shows the SRF overplot between MERSI and MODIS. According to the band spectral consistency, proper band-pairs between MERSI and MODIS are used in comparison. MERSI bands 1–4, 6–10, and 16–18 are cross-compared with MODIS. Fig. 6 shows the TOA apparent reflectance scatter plot between recalibrated FY-3B MERSI and Aqua MODIS in February 2011 from fifteen 5-min granules, in which the linear fitting parameters are shown. Relatively good consistency is obtained, with R^2 nearly 1.0 and the slopes within 1 ± 0.05 from linear correlation analysis. The bias statistics between MERSI and MODIS are listed in Table IX. The difference between MERSI TOA reflectance and that of MODIS is relatively small at MERSI bands 1, 9, 10, 16, and 18, with the relative bias $(\text{mean} \pm \sigma)$ nearly within 7%. The relatively large Std for band 16 is mainly due to the limited dynamic range of the samples, all with low TOA reflectance less than 0.01. The relative bias $(\text{mean} \pm \sigma)$ between MERSI and MODIS at MERSI bands 2, 3, 4, 6, and 8 are nearly within 10%. The uncertainties of the MERSI SRFs, detector uniformity, and sensor response stability may contribute to the bias, as well as the SRF difference between MODIS and MERSI. The bias is relatively large for MERSI bands 7 and 17, which are influenced by water-vapor absorption.

B. Prelaunch Calibration-Coefficient Usability

Before launch, FY-3B MERSI was calibrated using an integrating sphere in the laboratory and outdoor solar radiation-based calibration, which is similar as the SeaWiFS method [24], conducted by the vendor in 2009 at Dali, Yunnan Province. The laboratory calibration is mainly used to get the appropriate gain settings while the outdoor calibration produces the calibration coefficients by using a set of reference Spectralon panels to obtain the reflected solar source radiation. Table X lists the comparison result between the prelaunch calibration coefficients and the postlaunch initial coefficients of the daily calibration updating model for FY-3B MERSI. Bands 6 and 7 are not discussed here for their abnormal working status. It

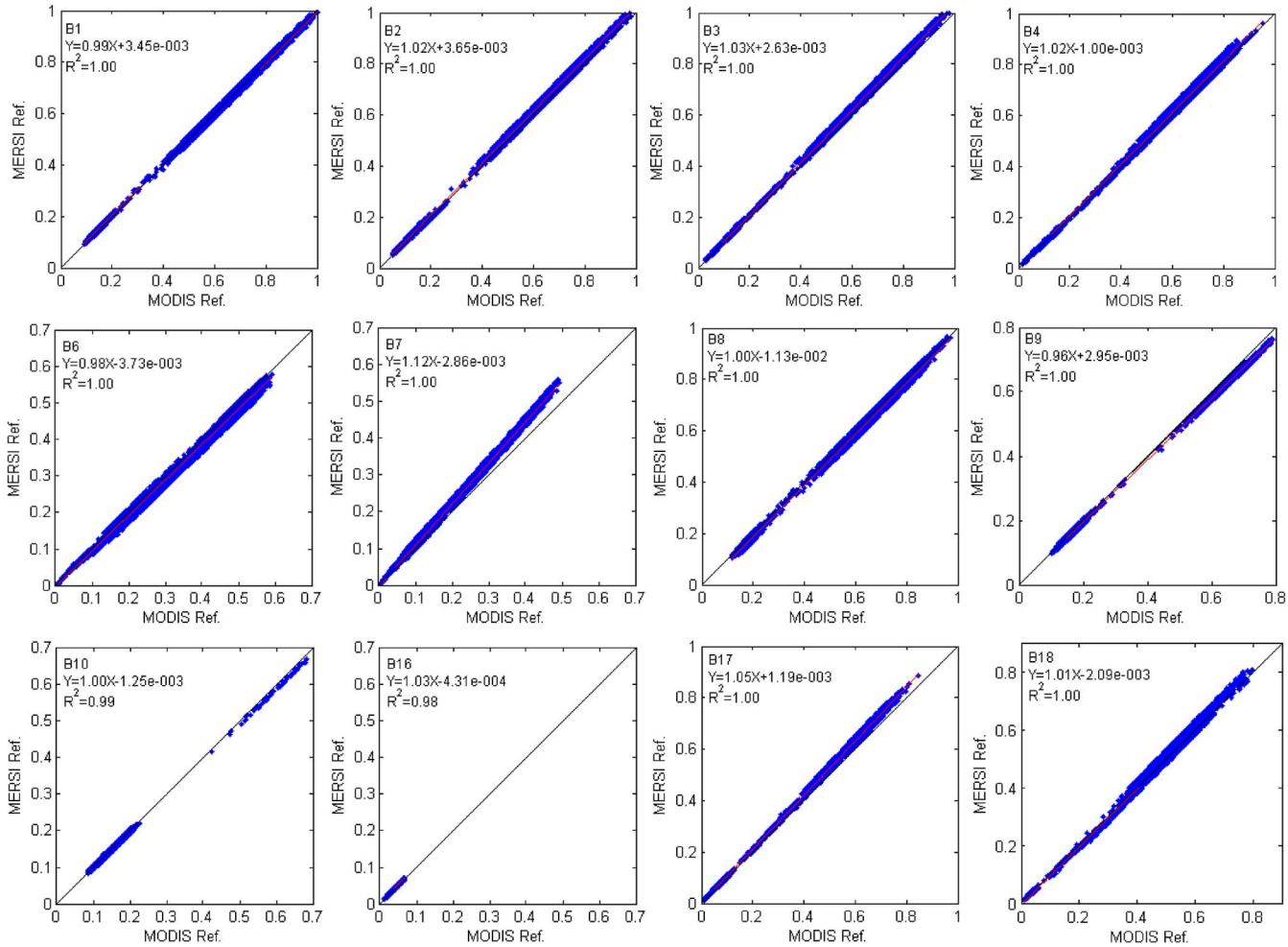

Fig. 6. TOA apparent reflectance scatter plot between recalibrated FY-3B MERSI using daily updating model and Aqua MODIS in February 2011.

TABLE IX
NEAR-SNO COMPARISON RESULTS BETWEEN RECALIBRATED FY-3B MERSI AND AQUA MODIS IN FEBRUARY 2011

MERSI Band (CW)	MODIS Band (CW)	PDif(%) m±σ	Ratio m±σ
1 (0.470)	3 (0.469)	1.33±2.46	1.01±0.02
2 (0.550)	4 (0.555)	5.05±4.58	1.05±0.05
3 (0.650)	1 (0.645)	6.29±3.99	1.06±0.04
4 (0.865)	2 (0.858)	3.61±6.01	1.04±0.06
6 (1.640)	6 (1.640)	-4.44±4.44	0.96±0.04
7 (2.130)	7 (2.130)	9.89±5.27	1.10±0.05
8 (0.412)	8 (0.412)	-6.00±4.77	0.94±0.05
9 (0.443)	9 (0.443)	-2.25±2.34	0.98±0.02
10 (0.490)	10 (0.488)	-0.58±2.44	0.99±0.02
16 (0.865)	16 (0.869)	1.16±6.13	1.01±0.06
17 (0.905)	17 (0.905)	8.66±5.87	1.09±0.06
18 (0.940)	19 (0.940)	-1.25±4.52	0.99±0.05

CW: Center wavelength in μm;
m: Mean; σ: Standard deviation;
PDif: $(Ref_{MERSI} - Ref_{MODIS})/Ref_{MODIS}$;
Ratio: Ref_{MERSI}/Ref_{MODIS}.

shows that the prelaunch calibration coefficients are obviously less than those of postlaunch initials for most bands and the relative bias between them exceeds 4% at most bands with the largest bias at band 8 of 17%. Thus, the prelaunch calibration coefficients could not be used after launch.

The primary uncertainties in the outdoor calibration are the downward direct radiation and reflectance of reference panels. Clear-sky conditions are required with a very low aerosol loading, so that the reflective direct solar radiation could be accurately calculated. There are also some risks associated with the outdoor method, e. g., sensor-optical-component contamination when exposed to environment. To improve the reliability of the prelaunch calibration, more strict calibration process should be performed, and reliable laboratory calibration should play an important role.

VI. SUMMARY AND CONCLUSION

MERSI is the keystone instrument onboard FY-3. After FY-3A MERSI launched in May 27, 2008, FY-3B MERSI was launched in November 5, 2010. Unfortunately, the antifouling cover of space radiant cooler was not successfully opened. Thus, the SWIR bands 6 and 7 have been operating in abnormal working conditions without radiant cooler since January 21, 2011.

The annual VC based on synchronous *in situ* measurements at the Dunhuang site used to be the baseline calibration method for MERSI RSBs. A multisite calibration tracking method has been developed for the effective monitoring of sensor response

TABLE X
COMPARISON BETWEEN PRELAUNCH CALIBRATION COEFFICIENTS AND POSTLAUNCH INITIALS (DSL = 0)

Band	Pre-launch	Post-launch	PDif (%)	Band	Pre-launch	Post-launch	PDif (%)
1	0.0259	0.0278	7.27	12	0.02015	0.0218	8.13
2	0.02562	0.0283	10.52	13	0.0203	0.0217	6.71
3	0.02578	0.0278	7.93	14	0.02021	0.0191	-5.39
4	0.02562	0.0288	12.45	15	0.02024	0.0206	1.86
6	0.01661	0.0218	31.20	16	0.02042	0.0220	7.82
7	0.00441	0.0180	308.79	17	0.02284	0.0222	-2.81
8	0.02002	0.0235	17.40	18	0.02277	0.0189	-16.84
9	0.02008	0.0219	9.17	19	0.02244	0.0226	0.90
10	0.0202	0.0211	4.46	20	0.02262	0.0254	12.42
11	0.02005	0.0215	7.01				

PDif: $(\text{Slope}_{\text{post-launch}}\text{-Slope}_{\text{pre-launch}})/\text{Slope}_{\text{pre-launch}}$;
The unit for the calibration slope is %/DN.

degradation and in-flight calibration-coefficient updating. FY-3B MERSI RSB postlaunch daily calibration updating model has been established based on the multisite calibration tracking with the annual Dunhuang site VC correction.

The reflectance calibration uncertainties for MERSI Dunhuang VC are within 3% for most bands. The MERSI calibration reference of Dunhuang VC has been evaluated against the observations of Aqua MODIS, showing the relative biases within 4% for window bands with wavelengths less than 1 μm. To further improve the accuracy of the Dunhuang VC, the surface BRDF and atmospheric aerosol properties should be modeled with more *in situ* measurements, and real-time ozone measurements should be also performed.

Based on radiative transfer modeling over stable sites without synchronous *in situ* measurements, the multisite calibration tracking method could produce the calibration coefficients time series. It is found by the long-term trending analysis that the shortwave channels of MERSI experience large degradation, particularly the 412-nm band with an annual degradation rate of approximately 18%, while most red and near-infrared bands are relatively stable with annual degradation rates within $\pm 1\%$.

The MERSI postlaunch daily calibration updating model has been established based on the long-term trend from multisite calibration tracking and Dunhuang VC correction. The recalibrated MERSI data have been validated against MODIS by near-SNO analysis, and good agreement has been achieved. Although this cross analysis is primary without spectral correction of the SRF difference, it gives the useful FY-3B MERSI radiometric performance information relative to Aqua MODIS. This calibration updating model could correct the on-orbit response change timely, and the validation results indicate that it is acceptable for fulfilling the MERSI calibration accuracy requirement of 7%.

Postlaunch calibration results also revealed that the prelaunch calibration coefficients have large bias. To improve the reliability of the prelaunch calibration, more strict calibration process, including sensor-optical-component protection from contamination, should be performed. The reliable absolute calibration at the laboratory should also play a more important role at the prelaunch phase.

ACKNOWLEDGMENT

The authors would like to thank T. Zhang for his help in the MERSI data preparation.

REFERENCES

[1] C. Dong, J. Yang, W. Zhang, Z. Yang, N. Lu, J. Shi, P. Zhang, Y. Liu, and B. Cai, "An overview of a new Chinese weather satellite FY-3A," *Bull. Amer. Meteorol. Soc.*, vol. 90, no. 10, pp. 1531–1544, Oct. 2009.

[2] X. Xiong, J. Sun, X. Xie, W. L. Barnes, and V. V. Salomonson, "On-orbit calibration and performance of Aqua MODIS reflective solar bands," *IEEE Trans. Geosci. Remote Sens.*, vol. 48, no. 1, pp. 535–546, Jan. 2010.

[3] Y. Zhang, K. Qiu, and X. Hu, "Vicarious radiometric calibration of satellite FY-1D sensors at visible and near infrared channels," *Acta Meteorol. Sinica*, vol. 18, no. 4, pp. 505–516, Jul. 2004.

[4] S. F. Biggar, K. J. Thome, and W. Wisniewski, "Vicarious radiometric calibration of EO-1 sensors by reference to high-reflectance ground targets," *IEEE Trans. Geosci. Remote Sens.*, vol. 41, no. 6, pp. 1174–1179, Jun. 2003.

[5] Y. J. Kaufman and B. N. Holben, "Calibration of the AVHRR visible and near-IR bands by atmospheric scattering, ocean glint and desert reflection," *Int. J. Remote Sens.*, vol. 14, no. 1, pp. 21–52, Jan. 1993.

[6] Y. M. Govaerts, M. Clerici, and N. Clerbaux, "Operational calibration of the Meteosat radiometer VIS band," *IEEE Trans. Geosci. Remote Sens.*, vol. 42, no. 9, pp. 1900–1914, Sep. 2004.

[7] A. Okuyama, T. Hashimoto, R. Nakayama, Y. Tahara, T. Kurino, H. Takenaka, S. Fukuda, T. Y. Nakajima, A. Higurashi, M. Sekiguchi, T. Takamura, and T. Nakajima, "Geostationary imager visible channel recalibration," in *Proc. EUMETSAT Meteorol. Satellite Conf. CD*, Sep. 2009, pp. 1–8.

[8] C. R. N. Rao and J. Chen, "Revised post-launch calibration of the visible and near-infrared channels of the Advanced Very High Resolution Radiometer (AVHRR) on the NOAA-14 spacecraft," *Int. J. Remote Sens.*, vol. 20, no. 18, pp. 3845–3491, Dec. 1999.

[9] X. Wu, J. T. Sullivan, and A. K. Heidinger, "Operational calibration of the Advanced Very High Resolution Radiometer (AVHRR) visible and near-infrared channels," *Can. J. Remote Sens.*, vol. 36, no. 5, pp. 602–616, Oct. 2010.

[10] N. G. Loeb, "In-flight calibration of NOAA AVHRR visible and near-IR bands over Greenland and Antarctica," *Int. J. Remote Sens.*, vol. 18, no. 3, pp. 477–490, Feb. 1997.

[11] W. R. Tahnk and J. A. Coakley, "Updated calibration coefficients for NOAA-14 AVHRR channels 1 and 2," *Int. J. Remote Sens.*, vol. 22, no. 15, pp. 3053–3057, Oct. 2001.

[12] D. R. Doelling, G. Hong, D. Morstad, R. Bhatt, A. Gopalan, and X. Xiong, "The characterization of deep convective cloud albedo as a calibration target using MODIS reflectances," in *Proc. SPIE*, Oct. 2010, vol. 7862, p. 786 20I.

[13] B.-J. Sohn, S.-H. Ham, and P. Yang, "Possibility of the visible-channel calibration using deep convective clouds overshooting the TTL," *J. Appl. Meteorol. Climatol.*, vol. 48, no. 11, pp. 2271–2283, Nov. 2009.

[14] W. Barnes, X. Xiong, R. Eplee, J. Sun, and C.-H. Lyu, "Use of the Moon for calibration and characterization of MODIS, SeaWiFS, and VIRS," in *Earth Science Satellite Remote Sensing: Vol. 2: Data, Computational Processing, and Tools*, J. J. Qu, W. Gao, M. Kafatos, R. E. Murphy, and V. V. Salomonson, Eds. New York: Springer-Verlag, 2006, pp. 98–119.

[15] C. Cao, E. Vermote, and X. Xiong, "Using AVHRR lunar observations for NDVI long-term climate change detection," *J. Geophys. Res.*, vol. 114, no. 20, p. D20 105, Oct. 2009.

[16] A. K. Heidinger, C. Cao, and J. T. Sullivan, "Using moderate resolution imaging spectrometer (MODIS) to calibrate Advanced Very High Resolution Radiometer reflectance channels," *J. Geophys. Res.*, vol. 107, no. D23, p. 4702, Dec. 2002.

[17] J.-J. Liu, Z. Li, Y.-L. Qiao, Y.-J. Liu, and Y.-X. Zhang, "A new method for cross-calibration of two satellite sensors," *Int. J. Remote Sens.*, vol. 25, no. 23, pp. 5267–5281, Dec. 2004.

[18] X. Hu, J. Liu, L. Sun, Z. Rong, Y. Li, Y. Zhang, Z. Zheng, R. Wu, L. Zhang, and X. Gu, "Characterization of CRCS Dunhuang test site and vicarious calibration utilization for FengYen (FY) series sensors," *Can. J. Remote Sens.*, vol. 36, no. 5, pp. 566–582, Oct. 2010.
[19] D. K. Clark, H. R. Gordon, K. J. Voss, Y. Ge, W. Broenkow, and C. Trees, "Validation of atmospheric correction over the oceans," *J. Geophys. Res.*, vol. 102, no. D14, pp. 17 209–17 217, Jul. 1997.
[20] C. B. Schaaf, F. Gao, A. H. Strahler, W. Lucht, X. Li, T. Tsang, N. C. Strugnell, X. Zhang, Y. Jin, J. P. Muller, P. Lewis, M. Barnsley, P. Hobson, M. Disney, G. Roberts, M. Dunderdale, C. Doll, R. P. d'Entremont, B. Hu, S. Liang, J. L. Privette, and D. Roy, "First operational BRDF, albedo nadir reflectance products from MODIS," *Remote Sens. Environ.*, vol. 83, no. 1/2, pp. 135–148, Nov. 2002.
[21] L. A. Remer, Y. J. Kaufman, D. Tanre, S. Mattoo, D. A. Chu, J. V. Martins, R.-R. Li, C. Ichoku, R. C. Levy, R. G. Kleidman, T. F. Eck, E. Vermote, and B. N. Holben, "The MODIS aerosol algorithm, products and validation," *J. Atmos. Sci.*, vol. 62, no. 4, pp. 947–973, Apr. 2005.
[22] R. McPeters, M. Kroon, G. Labow, E. Brinksma, D. Balis, I. Petropavlovskikh, J. P. Veefkind, P. K. Bhartia, and P. F. Levelt, "Validation of the aura ozone monitoring instrument total column ozone product," *J. Geophys. Res.*, vol. 113, no. 15, p. D15 S14, May 2008.
[23] E. Kalnay, M. Kanamitsu, R. Kistler, W. Collins, D. Deaven, L. Gandin, M. Iredell, S. Saha, G. White, J. Woollen, Y. Zhu, M. Chelliah, W. Ebisuzaki, W. Higgins, J. Janowiak, K. C. Mo, C. Ropelewski, J. Wang, A. Leetmaa, R. Reynolds, R. Jenne, and D. Joseph, "The NCEP/NCAR 40-year reanalysis project," *Bull. Amer. Meteorol. Soc*, vol. 77, no. 3, pp. 437–472, Mar. 1996.
[24] R. A. Barnes, R. E. Eplee, G. M. Schmidt, F. S. Patt, and C. R. McClain, "Calibration of SeaWiFS. I. Direct techniques," *Appl. Opt.*, vol. 40, no. 36, pp. 6682–6700, Dec. 2001.

Ling Sun received the M.S. degree in signal and information processing from Qingdao Ocean University, Qingdao, China, in 2002 and the Ph.D. degree in physical oceanology from the Chinese Academy of Sciences, Qingdao, in 2005.

She has been an Associate Professor since 2008 and the Agency Chief of the Calibration/Validation (CAL/VAL) Branch of the Satellite Meteorological Institute since 2011 with the National Satellite Meteorological Center, China Meteorological Administration, Beijing, China. She has been the Product Scientist of the FengYun-3 project for ocean color and aerosol over ocean since 2006. She is currently working on the optical instrument calibration and validation at visible bands. Her research interests include calibration and validation for optical sensors, and remote sensing of ocean color and aerosol.

Xiuqing Hu received the B.S. degree in atmospheric science from Nanjing University, Nanjing, China, in 1996 and the M.S. degree in cartography and geographical information system from Beijing Normal University, Beijing, China, in 2004. He has received the Ph.D. degree in quantitative remote sensing science from the Institute of Remote Sensing Application, Chinese Academy of Sciences, Beijing, China, in 2012.

From 1996 to 2004, he was a Research Assistant with the National Satellite Meteorological Center, China Meteorological Administration, Beijing, where he has been an Associate Professor and the Chief of the CAL/VAL Branch of the Satellite Meteorological Institute since 2004. He has been a Professor of engineering since 2010 and has been the Instrument Scientist of the MEdium Resolution Spectral Imager (MERSI) onboard FengYun-3 since 2006. He is currently a Visiting Scientist and also a Contractor with National Oceanic and Atmospheric Administration/NOAA Environmental Satellite, Data, and Information Service/Center for Satellite Applications and Research as a Remote Sensing Senior Scientist with Earth Resource Technology Inc. His research interests include calibration and validation for optical sensors, retrieval algorithms of aerosol/dust and water vapor, and climate data records from environment satellite.

Prof. Hu is a member of the Regional Steering Group, Sand and Dust Storm Warning Advisory and Assessment System, World Meteorological Organization, and of the Global Space-based Inter-Calibration System Research Working Group.

Na Xu received the Ph.D. degree in atmospheric physics and environment from the Chinese Academy of Sciences, Beijing, China, in 2010. Her thesis was on the modification and the application of atmospheric radiative transfer model.

She is currently a Research Assistant with the National Satellite and Meteorological Center, China Meteorological Administration, in Beijing. She is working on the vicarious calibration of FengYun satellite instruments.

Jingjing Liu received the B.S. degree in applied geophysics from Jilin University, Changchun, China, in 1984 and the M.S. degree in applied geophysics from the Beijing Research Institute of Uranium Geology, Beijing, China, in 1987.

In 2004, he was a Visiting Scholar with the University of Maryland, College Park, for one year. Since 2004, he has been a Professor with the National Satellite Meteorological Center, China Meteorological Administration, Beijing. His research interests include calibration and validation for optical sensors, retrieval algorithms, and *in situ* measurement methods of ground surface reflectance.

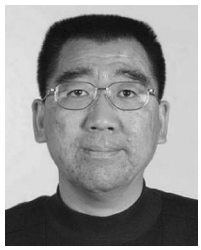

Lijun Zhang received the B.S. degree in computer software from Beijing Jiaotong University, Beijing, China, in 2007.

In 1995, he was an Engineer with the National Satellite Meteorological Center, China Meteorological Administration, Beijing, where he has been a Senior Engineer since 2011. He is responsible for instrument management of the laboratory of China Radiometric Calibration Sites and the indoor instrument calibration. He is experienced in field measurement for calibration and validation campaigns.

Zhiguo Rong received the B.S. degree in astronomic science from Nanjing University, Nanjing, China, in 1985.

From 2004 to 2009, he was the Deputy Director of the Satellite Meteorological Institute, National Satellite Meteorological Center, China Meteorological Administration (NSMC/CMA), Beijing, China, where he has been a Professor of engineering since 2005. He participated in the constructions of FengYun (FY)-1 and FY-2 series satellites engineering, mainly focusing on the satellite data preprocessing. He was responsible for the intercalibration between FY-1 and National Oceanic and Atmospheric Administration satellites in FY-1A/B/C/D missions, and the onboard and field calibrations of FY-2A/B/C satellites. He was also in charge of the constructions of China Radiometric Calibration Sites. He is currently the Deputy Director of the Satellite Operational Administration and Technology Department, NSMC/CMA. His research interests include calibration and validation for optical sensors, and space weather research.